Applied Mathematical Modelling 39 (2015) 794–808

Contents lists available at ScienceDirect

Applied Mathematical Modelling

journal homepage: www.elsevier.com/locate/apm

# Primal mixed solution to unconfined seepage flow in porous media with numerical manifold method ☆

Hong Zheng [a,*], Feng Liu [b], Chunguang Li [b]

[a] Key Laboratory of Urban Security and Disaster Engineering, Ministry of Education, Beijing University of Technology, Beijing 100124, China
[b] State Key Laboratory of Geomechanics and Geotechnical Engineering, Institute of Rock and Soil Mechanics, Chinese Academy of Sciences, Wuhan 430071, China

ARTICLE INFO

*Article history:*
Received 15 July 2013
Received in revised form 16 April 2014
Accepted 4 July 2014
Available online 19 July 2014

*Keywords:*
Unconfined seepage problems
Free boundary problems
Numerical manifold method
Moving least squares interpolation

ABSTRACT

The major difficulty in the analysis of unconfined flow in porous media is that the free surface is unknown *a priori*, where the nonlinearity is even stronger than the unsaturated seepage analysis. There is much space for both the adaptive mesh methods and the fixed mesh methods to improve. In this study, firstly two variational principles fitted to the numerical manifold method (NMM) are formulated, each of which enforces the boundary conditions and the material interface continuity conditions. In the setting of the NMM together with the moving least squares (MLS) interpolation, then the discretization models corresponding to the variational formulations are built, which are utilized to locate the free surface and scrutinize the computational results respectively. Meanwhile, a novel approach is developed to update the free surface in iteration. With high accuracy and numerical stability but no need to remesh, the proposed procedure is able to accommodate complicated dam configuration and strong non-homogeneity, where internal seepage faces may develop, a seldom touched problem in the literature.



## 1. Introduction

Due to the importance in engineering and strong nonlinearity in mathematics, problems of seepage with free surfaces, called unconfined seepage problems, are paid extensive attention from both engineers and mathematicians. The unconfined seepage analysis belongs to geometrical nonlinearity, while the unsaturated seepage analysis belongs to material nonlinearity and needs more soil parameters or curves, some of which are hard to obtain, such as soil–water characteristic curves. But the former's nonlinearity is stronger than the latter, because usually the analysis domain in the unsaturated seepage analysis does not change in iteration.

The procedures developed for the unconfined seepage problems are diverse, including the adaptive mesh methods and the fixed mesh methods. The adaptive mesh methods are easy to understand in concept, but they usually have to remesh explicitly during iteration, leading to laborious mesh generation or adjustment. Unless a good initial guess of the free surface is set, the adaptive mesh methods are hard to converge if inhomogeneous soils or complicated configurations are present. Moreover, the seepage analysis is usually coupled with the stress analysis, where the different meshes for the seepage analysis and the stress analysis would incur great troubles. In the setting of the classical finite element method, as a result, the adaptive mesh methods appear to have a tendency to give way to the fixed mesh methods.

☆ Supported by National Natural Science Funds of China (Project No. 11172313).
* Corresponding author. Tel.: +86 27 8719 9226; fax: +86 27 8719 7386.
*E-mail address:* hzheng@whrsm.ac.cn (H. Zheng).

http://dx.doi.org/10.1016/j.apm.2014.07.007
0307-904X/

The fixed mesh methods, whether the residual flow procedure (RFP) [1] or the variational inequality methods [2,3], blur the dry domain and the wet domain. The free surface is automatically identified once the problem is solved out. Although the RFP formulation is heuristic, 2- and 3-dimensional numerical examples [4] have shown it is very effective. Besides, Westbrook [5] showed that the Alt inequality method and the RFP have much in common when the numerical schemes resulting from these views are examined. Recently, Zheng et al. [6] gave a variational inequality formulation to the RFP [1,7].

Comprehensive reviews of variational inequality methods for free surface seepage problems are given by Oden and Kikuchi [8] and Bruch [9]. By specifying the potential seepage surface as Signorini's boundary condition, Zheng et al. [10] proposed a new variational inequality formulation that eliminates singularity of the seepage point, mitigating the mesh dependence. Later on, Chen et al. [11] generalized the formulation to the non-steady seepage flow.

Rigorous as they are, the variational inequality methods require more mathematical training than the average engineer receives in his formal education. With maturity of the mesh-free methods, as a result, the idea in the adaptive mesh methods is adopted again to solve free boundary value problems including the unconfined seepage problems. We mention that some methods based on the finite element methods seemingly analyze the unconfined seepage problems on fixed meshes, such as [12], but they actually utilize the strategies of the adaptive mesh methods in calculating the contribution of those elements cut by the free surface to the flow matrix.

In addition to the finite element methods, some other numerical methods are also used in the unconfined seepage problems. These methods have their own strengths and weaknesses. For example, the finite volume method by Darbandi and Torabi [13] assures mass conservation over cells but requires that the grid match the free surface. Starting also from the mass conservation equation of integration form, the finite difference method by Bardet and Tobita [14] would encounter troubles in enforcing the boundary conditions if the problem domain is complicated in shape. Highly accurate as it is, the residual velocity method by Zhang and Jiang [15] is suited only for the situations where the free surface does not undergo drastic singularity or changes during iteration. With no need to pay much attention to the location of the free surface in iteration, the level-set method by Herreros et al. [16], has limited precision; and so on.

Now that the mesh fetters have been broken due to the development of the mesh-free methods, which are cut out for the free boundary problems including the unconfined flow problems. As far as we know, Li et al. [17], firstly adopted the Element-Free Galerkin Methods (EFGM) to solve unconfined seepage problems. In the procedure, they selected the moving least squares (MLS) method with singular weight functions, yielding the shape functions with interpolation property. Using the shape functions with interpolation property simply assures the satisfaction of the essential boundary condition at the boundary nodes but not on the whole essential boundary. From the results given in their paper, as a result, the solution precision is very limited and qualified only for homogeneous embankments. Besides, the nodes in the procedure usually have to be added or deleted during iteration. In principle, adding or deleting nodes in the EFGM is feasible. Nevertheless, it is not easy how to add nodes so that accuracy and numerical stability are guaranteed, because the configuration of nodes in the MLS has quite a salient effect on the accuracy of the function to be approximated, see examples given in [18].

To exploit the properties of the MLS, we formulate the variational forms of the unconfined seepage problem in the setting of the numerical manifold method (NMM) [19], where the mathematical cover (MC) is composed of the regularly-deployed nodes and the associated shape function supports. Considering the moving free surface in iteration might not match the regularly-deployed nodes, the proposed variational forms enforce both the essential boundary condition and the material interface continuity condition. So, the mesh adjustment is unnecessary during iteration.

As we know, another crux in the analysis of unconfined seepage flow is the treatment of free surfaces with singularity. For example, when a free surface penetrates a material interface that separates two media with quite different seepage properties, it will have an abrupt change, causing solution hard to converge. Even for a very neat problem as shown in Fig. 12(a) below, the results given by those popular procedures differ considerably from each other, with almost all having very large errors. In order to improve the convergence in treating singular free surfaces, a new strategy for updating the free surface in iteration is put forward. From the typical examples, it will be seen that not only is the strategy able to achieve very high accuracy, but the introduction of the NMM is necessary for treating those singular free surfaces as well. Besides, we also analyzed a practical seepage problem of an earth and rockfill dam, where an internal seepage face develops along the material interface between a sloping core and the rest of the dam. Such problems are frequently encountered in the seepage analysis of earth and rockfill dams, but seldom touched in the literature.

## 2. Numerical manifold space

We first recapitulate the numerical manifold method (NMM) invented by Shi [19]. Suppose $\Omega$ is the problem domain. To be clear, we confine ourselves to two dimensional cases. $\Omega$ may keep invariant as in most applications, may deform in space due to being loaded, or may have some internal or external free boundaries that are unknown *a priori*. Internal free boundaries arise in the elastic–plastic analysis, the unsaturated seepage analysis, and so on.

To fit itself to the uncertainty of $\Omega$, the NMM introduces two cover systems, what are referred to as the mathematical cover (MC) and the physical cover (PC), respectively. The MC is a collection of simply connected domains $\{M_i\}$, $i = 1, \ldots, m$, with each $M_i$ called a mathematical patch, and $m$ the number of all mathematical patches. $\{M_i\}$ must be large enough in size or sufficient in number to cover the whole $\Omega$. Using the components of $\Omega$, including the boundary, the material

interface and the discontinuity, to cut $M_i$, and discarding those outside $\Omega$, we obtain what are called physical patches, denoted by $P_{i-j}$, $j = 1, \ldots, n_i$, with $n_i$ the number of patches cut off from the same $M_i$. All $P_{i-j}$ constitute the PC.

Here is an example. Shown in Fig. 1 is the problem domain $\Omega$, containing a material interface AB and a reentrant angle K. Now let's cover $\Omega$ with three mathematical patches, $M_1$ – a big cycle, $M_2$ – a small cycle, and $M_3$ – a rectangle. Then, we use $\Omega$'s components to cut $M_1$, and obtain two physical patches $P_{1-1}$ and $P_{1-2}$ illustrated in Fig. 2. Proceeding such as this, we create other two groups of physical patches shown in Figs. 3 and 4, respectively.

According to the partition of unity theorem [20], we can always construct a collection of weight functions, $\{N_i(\boldsymbol{r})\}$, satisfying

$$N_i(\boldsymbol{r}) = 0, \quad \text{if } \boldsymbol{r} \notin M_i; \tag{1.1}$$

$$0 \le N_i(\boldsymbol{r}) \le 1, \quad \text{if } \boldsymbol{r} \in M_i; \tag{1.2}$$

$$\sum_{i=1}^{n} N_i(\boldsymbol{r}) = 1, \quad \text{if } \boldsymbol{r} \in \Omega. \tag{1.3}$$

$\{N_i(\boldsymbol{r})\}$ is collectively called the partition of unity subordinate to the MC $\{M_i\}$, and each $N_i(\boldsymbol{r})$ can be made arbitrarily smooth.

By restricting $\{N_i(\boldsymbol{r})\}$ subordinate to the MC $\{M_i\}$ onto the PC $\{P_{i-j}\}$, we obtain the partition of unity $\{N_{i-j}(\boldsymbol{r})\}$ subordinate to the PC $\{P_{i-j}\}$. Therefore, all $P_{i-j}$ generated from the same patch $M_i$ may have the same expression as $N_i(\boldsymbol{r})$ if they are not separated during solution. Because $N_{i-j}(\boldsymbol{r})$ vanishes outside $P_{i-j}$, $P_{i-j}$ is also said to be the support of $N_{i-j}(\boldsymbol{r})$.

To be convenient for statements and programming, we code all $P_{i-j}$ and $N_{i-j}(\boldsymbol{r})$ with single subscripts, and denote them by $P_k$ and $N_k(\boldsymbol{r})$, respectively, $k = 1, \ldots, n$, with $n$ being the number of all physical patches.

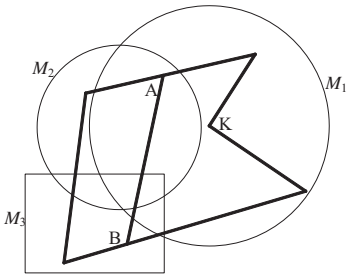


**Fig. 1.** Problem domain and mathematical cover.

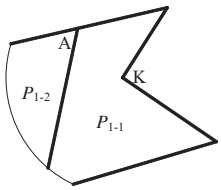


**Fig. 2.** Two patches $P_{1-1}$ and $P_{1-2}$ from $M_1$.

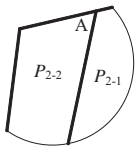


**Fig. 3.** Two patches $P_{2-1}$ and $P_{2-2}$ from $M_2$.

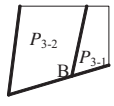


**Fig. 4.** Two patches $P_{3-1}$ and $P_{3-2}$ from $M_3$.

To this point, the most salient difference between the NMM and the partition of unity method (PUM) [21] is that the cover in the NMM can be variable both in shape and in topology; while in the PUM the cover is variable only in shape. The initial cover (the physical cover, actually) in the NMM is generated from a predefined mathematical cover. Then, the physical cover may change as $\Omega$ evolves. The changes of the physical cover include deformation in shape, and separation due to the breakage of $\Omega$ (leading to topological change of the physical cover). Since the predefined mathematical cover is deemed full of the whole space, whenever necessary, the physical cover can be recreated from the mathematical cover so as to guarantee the interpolation accuracy in solution. It is the introduction of the two separate cover systems that facilitates the solution of continuous and discontinues deformation in a unified context, and simplifies the treatment of drastic singularity in the free surface. We will see this in example 7.2.

On each physical patch $P_i$ we define a function space, called the patch space $V_i(P_i)$. Each function in $V_i$, called a patch function, should reflect as far as possible the local behavior of the solution on $P_i$. For example, the patch $P_{1-1}$, see Fig. 2, contains the reentrant angle K. Near the point K the solution has some singularity dependent on the magnitude of the reentrant angle. Then, the patch functions on $P_{1-1}$ should better include such singularity. In case that the asymptotic behavior of the solution on patch $P_i$ is not familiar to us, a natural choice for $V_i$ is the polynomial space, while zero-degree polynomials, i.e., constants, are the most frequently selected.

The test or trial space over the problem domain $\Omega$ in the Galerkin variational formulation, called the NMM space and denoted by $V(\Omega)$, is constructed by pasting together all patch spaces $V_i$ through the partition of unity $\{N_i(\boldsymbol{r})\}$, as follows

$$V(\Omega) = \sum_{i=1}^{n} N_i V_i \equiv \left\{ \sum_{i=1}^{n} N_i v_i \,\middle|\, v_i \in V_i \right\}. \tag{2}$$

We mention that the NMM space in the form of Eq. (2) is actually the Lagrange form that is usually fit for the second-order problems. For the fourth-order problems, we should take the NMM space of the Hermite form, see [22] for details.

In principle, the construction of mathematical covers is diverse. However, almost all applications and developments of the NMM in the literature create their mathematical covers from the finite element meshes, see [23–25] for details. To get rid of constraints from the finite element meshes, in this study the mathematical cover consists of all the supports of MLS-based shape functions, which can be referred to [18] for the construction.

## 3. Description of the problem in PDE form

Without loss of generality, as an example, we take the seepage flow of a soil dam illustrated in Fig. 5, in which water is considered to flow only in the saturated domain, not taking into account the capillarity effects as in [26]. Compared with the unconfined seepage analysis, the unsaturated seepage analysis is weaker in nonlinearity because it has no issue of shifting the free surface. But the unsaturated seepage analysis needs more soil parameters that are obtained by quite sophisticated experiments. The results based on the saturated seepage assumption usually satisfy the requirements in the stability analysis of soil dams. Therefore, the saturated seepage analysis has been playing a major role in dam and embankment engineering. In addition, the free surface resulting from the saturated seepage analysis can be made more practical through a correction proposed by Parlange and Brutsaert [27].

The total head at a point in the flow domain $\Omega_w$ is defined as

$$\phi = y + p/\gamma_w, \quad (\text{in } \Omega_w), \tag{3}$$

in which $y$ is the ordinate, $p$ the pore water pressure, and $\gamma_w$ the unit weight of water.

Suppose that in the flow domain $\Omega_w$ Darcy's law is satisfied

$$\boldsymbol{v} = \boldsymbol{D}\boldsymbol{i}. \tag{4}$$

Here, $\boldsymbol{D}$ is the permeability tensor of second order; and $\boldsymbol{i}$ is the hydraulic gradient defined by

$$\boldsymbol{i} = -\nabla\phi, \tag{4.1}$$

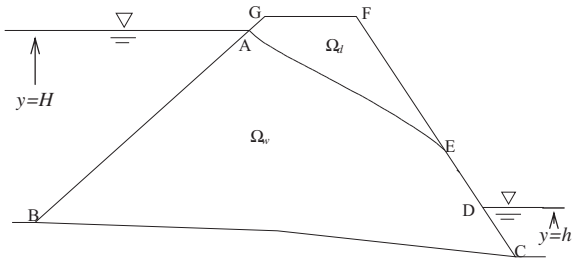


**Fig. 5.** Schematic for unconfined seepage.

with $\nabla$ the gradient operator.

The flow of water in $\Omega_w$ obeys the equation of continuity

$$\nabla \cdot \boldsymbol{v} = 0, \quad (\text{in } \Omega_w), \tag{5}$$

and the boundary conditions as follows.

The water head boundary condition

$$\phi = \bar{\phi}, \quad (\text{on } \Gamma_\phi = \text{AB} + \text{CD}), \tag{5.1}$$

where $\bar{\phi}$ equals $H$ on the upstream surface AB and $h$ on the downstream surface CD, with $H$ and $h$ being the ordinates of the water levels, respectively, see Fig. 5.

The flux boundary condition

$$\boldsymbol{n}^T \boldsymbol{v} = 0, \quad (\text{on } \Gamma_q = \text{BC}), \tag{5.2}$$

in which $\boldsymbol{n}$ denotes the unit normal outward vector of the boundary.

The boundary condition on the free surface

$$\begin{cases} \phi = y \\ \\ \boldsymbol{n}^T \boldsymbol{v} = 0 \end{cases} \quad (\text{on } \Gamma_f = \text{AE}). \tag{5.3}$$

The boundary condition on the seepage surface

$$\phi = y \quad (\text{on } \Gamma_s = \text{DE}). \tag{5.4}$$

The continuity condition on the material interface

$$\begin{cases} \phi^+ = \phi^- \\ \\ \boldsymbol{n}^T \boldsymbol{v}^+ = \boldsymbol{n}^T \boldsymbol{v}^- \end{cases} \quad (\text{on } \Gamma_m), \tag{5.5}$$

where the subscripts "+" and "−" refer to the quantities on $\Gamma_m$ but belonging to the two distinct domains adjoining along $\Gamma_m$, respectively.

If all the above conditions are satisfied, we can prove that

$$\boldsymbol{n}^T \boldsymbol{v} \geq 0, \quad (\text{on } \Gamma_s = \text{DE}), \tag{5.6}$$

see [10] for details.

Since the free surface $\Gamma_f$ is unknown *a priori*, to locate $\Gamma_f$ is a primary goal in the seepage analysis.

## 4. The primal mixed variational formulation

Given $\Omega_w$, we can construct two variational formulations associated with the above PDE formulation, where the free surface $\Gamma_f$ is regarded as the flux boundary and the water head boundary, respectively. Regarding $\Gamma_f$ as the flux boundary leads to the functional

$$\pi^1(\phi, q_n) = \sum_k \int_{\Omega_k} \frac{1}{2} \boldsymbol{i}^T \boldsymbol{v} d\Omega + \int_{\Gamma_\phi^1} (\phi - \bar{\phi}) q_n dS + \int_{\Gamma_m} (\phi^+ - \phi^-) q_n dS, \tag{6}$$

where $\Gamma_\phi^1 = \Gamma_\phi + \Gamma_s$, with $\bar{\phi} = y$ on $\Gamma_s$.

Regarding $\Gamma_f$ as the water head boundary gives the functional

$$\pi^2(\phi, q_n) = \sum_k \int_{\Omega_k} \frac{1}{2} \boldsymbol{i}^T \boldsymbol{v} d\Omega + \int_{\Gamma_\phi^2} (\phi - \bar{\phi}) q_n dS + \int_{\Gamma_m} (\phi^+ - \phi^-) q_n dS, \tag{7}$$

where $\Gamma_\phi^2 = \Gamma_\phi + \Gamma_s + \Gamma_f$, with $\bar{\phi} = y$ on $\Gamma_s + \Gamma_f$. We note that $\boldsymbol{i}$ and $\boldsymbol{v}$ in $\pi^i$ are related to $\phi$ by Eqs. (5) and (4) respectively.

It can be proved that

$$\delta \pi^i(\phi, q_n) = 0, \tag{8}$$

for $i = 1, 2$, is equivalent to the PDE formulation in the preceding section. Since both the primal function $\phi$ and the gradient-based function $q_n$ are independent, the two formulations given by Eq. (8) are primal mixed formulations.

What differs from the conventional primal formulation is that all the essential conditions in the primal formulation, including the water head boundary condition and the interface continuity condition, become the natural conditions in both $\pi^1$ and $\pi^2$. Here are two reasons for us to propose the two primal mixed formulations. On the one hand, in general the MLS-based shape functions do not have the delta property. On the other hand, even if the MLS-based shape functions have the delta property, the nodes do not necessarily match the problem domain. To guarantee the interpolation precision and to

consider the potential deformation of the problem domain, as stated subsequently, usually the NMM deploy regularly-distributed nodes in space and do not pay too much attention to the details of the problem domain, causing the nodes might not match the problem domain. The two reasons prohibit the essential boundary conditions from being enforced directly.

As an aside, in the NMM the solution precision is totally determined by the configuration of the mathematical cover. Whether the nodes match the problem domain has little effect on the solution precision. This is considered another advantage of NMM over other numerical methods; see [22] for details.

Both the two variational formulations will be used subsequently. $\pi^1(\phi, q_n)$ is used to solve for $\phi$ and $q_n$, while $\pi^2(\phi, q_n)$ to check the accuracy of solutions.

**Proof.** Firstly, we calculate $\delta\pi^i(\phi, q_n)$

$$\delta\pi^i = \sum_k \int_{\Omega_k} \delta \boldsymbol{i}^T \boldsymbol{v} d\Omega + \int_{\Gamma_\phi^i} q_n \delta\phi dS + \int_{\Gamma_m} q_n(\delta\phi^+ - \delta\phi^-) dS + \int_{\Gamma_\phi^i} (\phi - \bar{\phi})\delta q_n dS + \int_{\Gamma_m} (\phi^+ - \phi^-)\delta q_n dS. \quad \square \tag{9}$$

Using the identity for a typical material domain $\Omega_k$,

$$\int_{\Omega_k} \delta \boldsymbol{i}^T \boldsymbol{v} d\Omega = -\int_{\Omega_k} (\nabla(\delta\phi))^T \boldsymbol{v} d\Omega = \int_{\Omega_k} (\delta\phi)\nabla \cdot \boldsymbol{v} d\Omega - \int_{\partial\Omega_k} (\boldsymbol{n}^T \boldsymbol{v})\delta\phi d\Omega,$$

and considering

$$\partial\Omega_k = \Gamma_\phi^{ik} + \Gamma_q^{ik} + \Gamma_m^k, \quad \sum_k \Gamma_\phi^{ik} = \Gamma_\phi^i, \quad \sum_k \Gamma_q^{ik} = \Gamma_q^i, \quad \text{and} \quad \sum_k \Omega_k = \Omega_w,$$

with

$$\Gamma_q^{ik} = \begin{cases} \Gamma_q^k + \Gamma_f^k, & i = 1 \\ \Gamma_q^k, & i = 2 \end{cases},$$

and

$$\Gamma_q^i = \begin{cases} \Gamma_q + \Gamma_f, & i = 1 \\ \Gamma_q, & i = 2 \end{cases},$$

and

$$\sum_k \int_{\Gamma_m^k} (\boldsymbol{n}^T \boldsymbol{v})\delta\phi dS = \int_{\Gamma_m} [(\boldsymbol{n}^T \boldsymbol{v}^+)\delta\phi^+ - (\boldsymbol{n}^T \boldsymbol{v}^-)\delta\phi^-] dS,$$

due to $\boldsymbol{n} = \boldsymbol{n}^+ = -\boldsymbol{n}^-$, the first item of the right hand of Eq. (9) becomes

$$\sum_k \int_{\Omega_k} (\delta \boldsymbol{i})^T \boldsymbol{v} d\Omega = \int_{\Omega_w} (\delta\phi)\nabla \cdot \boldsymbol{v} d\Omega - \int_{\Gamma_q^i} (\boldsymbol{n}^T \boldsymbol{v})\delta\phi dS - \int_{\Gamma_\phi^i} (\boldsymbol{n}^T \boldsymbol{v})\delta\phi dS - \int_{\Gamma_m} [(\boldsymbol{n}^T \boldsymbol{v}^+)\delta\phi^+ - (\boldsymbol{n}^T \boldsymbol{v}^-)\delta\phi^-] dS. \tag{10}$$

Substituting Eq. (10) into Eq. (9), we have

$$\begin{aligned} \delta\pi^i = {} & \int_{\Omega_w} (\delta\phi)\nabla \cdot \boldsymbol{v} d\Omega - \int_{\Gamma_q^i} (\boldsymbol{n}^T \boldsymbol{v})\delta\phi dS + \int_{\Gamma_\phi^i} (q_n - \boldsymbol{n}^T \boldsymbol{v})\delta\phi dS + \int_{\Gamma_m} [(q_n - \boldsymbol{n}^T \boldsymbol{v}^+)\delta\phi^+ - (q_n - \boldsymbol{n}^T \boldsymbol{v}^-)\delta\phi^-] dS \\ & + \int_{\Gamma_\phi^i} (\phi - \bar{\phi})\delta q_n dS + \int_{\Gamma_m} (\phi^+ - \phi^-)\delta q_n dS. \end{aligned} \tag{11}$$

Putting $\delta\pi^i(\phi, q_n) = 0$, not only are equations from (5), (5.1)–(5.6) reproduced, but $q_n$ is recognized as the flux through a boundary point with normal $n$, that is to say,

$$q_n = \boldsymbol{n}^T \boldsymbol{v}, \quad \text{on} \quad \Gamma_\phi^i \quad \text{or} \quad \Gamma_m.$$

As a result, $q_n \geq 0$ on $\Gamma_s$ due to (5.6).

## 5. The numerical manifold formulation

We deploy the MLS nodes over the whole dam domain $\Omega$. These nodes do not have to match the boundary or the material interface, and they are even allowed to be outside $\Omega$, as long as they can influence $\Omega$. Hereafter, by "a node, say node-*i*, influences $\Omega$" we mean "the support of node-*i*'s shape function intersects with $\Omega$". Associated with node-*i* is the circle $M_i$ of finite diameter. Outside $M_i$ the node-*i*'s shape function vanishes. $M_i$ is accordingly called the support of the node-*i*'s shape function. The collection of all $M_i$ constitutes the mathematical cover of $\Omega$.

Now we cut all $M_i$ with the components of $\Omega_w$, including the assumed free surface, and obtain the physical cover, $\{P_k\}$. We denote by $\left\{N_\phi^k(\boldsymbol{r})\right\}$ the partition of unity subordinate to $\{P_k\}$. Actually, $\left\{N_\phi^k(\boldsymbol{r})\right\}$ are the shape functions of all nodes. Each patch $P_k$ is also referred to as the influence domain of node-$k$.

It should be pointed out that such a cutting operation is only in a theoretical sense, but actually no cutting operation is involved if the integrations in $\pi^i(\phi, q_n)$ are numerically calculated over a background net [28]. More specifically, whenever an $M_i$ is to be divided by a material interface $\Gamma_m$ into, say 2 patches belonging to two distinct material domains respectively, see Fig. 6(a), what we need to do is generate a new node index, say $i'$, and attach $i'$ to the newly generated patch $P_{i'}$ (the shadowed part in Fig. 6(b)). In this way, we have two nodal indices, $i$ (original) and $i'$ (newly generated), associated with the two distinct patches $P_i$ and $P_{i'}$ respectively, see Fig. 6(b). $P_{i'}$ and $P_i$ have the same center, but we never really form $P_{i'}$ but assign it a new nodal index $i'$. We call all these nodes for interpolating variable $\phi$ as $\phi$-nodes, including the original nodes and the newly generated nodes, each of which is associated with a physical patch. Consequently, the proposed procedure is easy and straightforward to implement.

By using $\left\{N_\phi^k(\boldsymbol{r})\right\}$, we approximate the water head $\phi$ in $\pi^i(\phi, q_n)$ by

$$\phi = \sum_k \phi_k N_\phi^k(\boldsymbol{r}), \tag{12}$$

with $\phi_k = \phi(\boldsymbol{r}_k)$ and $\boldsymbol{r}_k$ = position vector of node-$k$. For simplicity, here we take the functions in all patch spaces $V_k$ as constants. However, we mention that it is feasible and salutary to exploit the local behavior derived by Aalto [29] if higher precision is sought.

As for another independent variable $q_n$ defined on the material interface $\Gamma_m$ and the water boundary $\Gamma_\phi^i$ in $\pi^i(\phi, q_n)$ of Eqs. (6) and (7), we also deploy nodes, called $q$-nodes, on $\Gamma_m$ and $\Gamma_\phi^i$, with the same density as the $\phi$-nodes. With the $q$-nodes, we approximate $q_n$ by

$$q_n = \sum_j q_n^j N_q^j(\boldsymbol{r}), \tag{13}$$

with $N_q^j(\boldsymbol{r})$ being piecewise linear interpolant of the $q$-node indexed by $j$.Substituting equations (12) and (13) into Eq. (9) and putting $\delta\pi^i(\phi, q_n) = 0$, we have its NMM formulation

$$\begin{bmatrix} \boldsymbol{K} & \boldsymbol{C} \\ \boldsymbol{C}^T & 0 \end{bmatrix} \begin{pmatrix} \boldsymbol{\varphi} \\ \boldsymbol{q} \end{pmatrix} = \begin{pmatrix} \boldsymbol{f}_\varphi \\ \boldsymbol{f}_q \end{pmatrix}, \tag{14}$$

where $\boldsymbol{\phi}$ = vector formed by $\phi$ of all relevant $\phi$-nodes; $\boldsymbol{q}$ = vector of $q_n$ of all $q$-nodes. The sub-matrices and vectors involved are defined as

$$\boldsymbol{K} = (K_{IJ}), \quad K_{IJ} = \int_\Omega \sum_{i,j} D_{ij} \frac{\partial N_\phi^I}{\partial x_i} \frac{\partial N_\phi^J}{\partial x_j} d\Omega, \tag{14.1}$$

$$\boldsymbol{C} = (C_{IK}), \quad C_{IK} = \begin{cases} \int_{\Gamma_\phi^i} N_\phi^I N_q^K dS, & \text{if node } K \in \Gamma_\phi^i \\ \operatorname{sgn}(I) \int_{\Gamma_m} N_\phi^I N_q^K dS, & \text{if node } K \in \Gamma_m \end{cases}, \tag{14.2}$$

$$\boldsymbol{f}_\phi = 0, \tag{14.3}$$

$$\boldsymbol{f}_q = \left(f_q^I\right), \quad f_q^I = \int_{\Gamma_\phi^i} N_q^I \bar{\phi} dS, \tag{14.4}$$

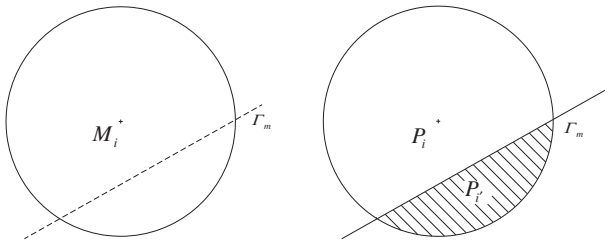


(a) Influence domain $M_i$ to be cut by $\Gamma_m$ (b) Two patches cut by $\Gamma_m$

**Fig. 6.** Two patches generated from node-$i$'s influence domain.

with

$$\mathrm{sgn}(I)=\begin{cases}+1, & \text{if} \quad I\in\Omega_m^+\\ -1, & \text{if} \quad I\in\Omega_m^-\end{cases}. \tag{14.5}$$

Here, $\Omega_m^+$ and $\Omega_m^-$ represent the two material domains separated by $\Gamma_m$ respectively.

Since all the boundary conditions and the continuity conditions on the material interface have turned into the natural conditions of $\delta\pi^i(\phi,q_n)=0$, we can directly solve system (14) with no need to introduce the boundary conditions.

The systems similar in form to Eq. (14) arise from many applications, and are usually called the KKT systems. In general, the flow matrix $\boldsymbol{K}$ in Eq. (14) has a rank deficiency of $r$, with $r$ being the number of distinct material domains in $\Omega_w$. Now there have been numerous algorithms for such systems. For example, Zheng and Li [30] developed an efficient and stable direct solver for the KKT system.

## 6. The update strategy for free surfaces

By regarding a potential free surface $\Gamma_f$ as the flux boundary, one solves numerically a boundary value problem for $\phi$. If $\phi\approx y$ on $\Gamma_f$, the iteration is terminated. Otherwise, one shifts $\Gamma_f$ in the vertical direction and repeats the process till $\phi\approx y$ on $\Gamma_f$. This is the update strategy proposed in most of the existing works; see [8] for example. By this procedure, one frequently has to discard some points on the moving free surface that go outside the problem domain, causing troubles in programming. Moreover, when the free surface has a nearly vertical segment, the solution is hard to converge unless extremely dense meshes are adopted.

For simplicity of the statements, hereafter solving $\delta\pi^1(\phi,q_n)=0$ refers actually to solving its discretized version, i.e., system (14).

To improve the robustness of updating the free surface, we propose the update strategy as follows.

(1) Determine a line segment representing the potential seepage face, say DF shown in Fig. 7, on which the exit point of the free surface will be. Then, find out the intersection H of the downstream line DF and the upstream line BG. Note that the entrance point A of the free surface is on the upstream surface BG.
(2) Select a point on the seepage face DF, say point E, as an initial guess of the exit point of the free surface, and then link points A and E, obtaining a line segment AE that will be viewed as an initial guess of the free surface.
(3) Divide the initial free surface AE into some intervals with distinct points $\mathrm{Q}_1,\mathrm{Q}_2,\ldots,\mathrm{Q}_s$.
(4) Link point H with points $\mathrm{Q}_1,\mathrm{Q}_2,\ldots,\mathrm{Q}_s$, obtaining a group of rays $\mathrm{HQ}_1,\mathrm{HQ}_2,\ldots,\mathrm{HQ}_s$. From now on, points $\mathrm{Q}_1,\mathrm{Q}_2,\ldots,\mathrm{Q}_s$, will move along these rays as the iteration proceeds.

Once the above preparation is finished, we solve $\delta\pi^1(\phi,q_n)=0$ for $\phi$ and $q_n$ with the assumed free surface AE. Then, we check if

$$\delta=\max_i|\delta_i|<\varepsilon, \tag{15}$$

holds. Here, $\varepsilon$ is the user-specified tolerance, and

$$\delta_i=\phi(\mathrm{Q}_i)-y(\mathrm{Q}_i), \tag{15.1}$$

$i=1,\ldots,s$. $\phi(\mathrm{Q}_i)$ is the value of water head at point $\mathrm{Q}_i$ calculated by Eq. (12), and $y(\mathrm{Q}_i)$ is the ordinate of point $\mathrm{Q}_i$. If Eq. (15) is satisfied, we terminate the solution. Otherwise, we move point $\mathrm{Q}_i$ along the ray $\mathrm{HQ}_i$ to point $\mathrm{Q}_i'$, as illustrated in Fig. 8. Here, $\mathrm{Q}_i'$ is the intersection of the ray $\mathrm{HQ}_i$ and the line $\mathrm{Q}_i'\mathrm{N}_i$ that passes point $\mathrm{N}_i$ and is parallel to the free surface's tangent at point $\mathrm{Q}_i$. Point $\mathrm{N}_i$ is on the same vertical line as $\mathrm{Q}_i$ but has a distinct ordinate as

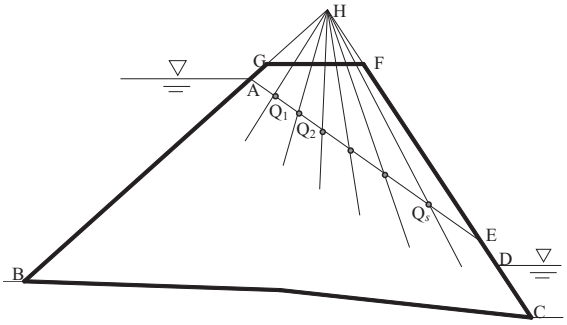


**Fig. 7.** Updating paths for the free surface.

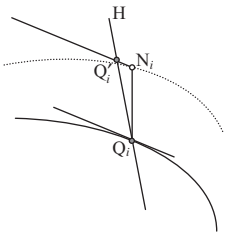


**Fig. 8.** Update to a point on the free surface.

$$y(N_i) = y(Q_i) + \omega\delta_i. \tag{16}$$

Here, $\omega$ is a scaling factor that will be explained subsequently.

Fig. 8 schematically illustrates the update to a typical point $Q_i$ on the current free surface (the solid line), where the dot line represents the new location of the free surface after the update. Clearly, the update process defined in the above guarantees that all initially deployed points on the free surface, $Q_1, Q_2, \ldots, Q_s$, are kept inside the dam domain during iteration, avoiding troubles in treating $Q_i$ going outside the dam domain.

The idea in the update strategy is that the variation of the free surface between two consecutive iterations is so small that the current point $Q_i$ and its update in the vertical direction, point $N_i$, see Fig. 8, have nearly parallel tangents. In order to guarantee the small variation of the free surface in two consecutive iterations, we stipulate the maximum vertical variation of the current free surface in the next iteration is not greater than a user-specified length $\rho$. Clearly, this can be readily implemented in this way. If $\delta \le \rho$, see Eq. (15) for the definition of $\delta$, let the scaling factor $\omega = 1$ in Eq. (16). Otherwise, let $\omega = \rho/\delta$. In general, $\rho$ can be given quite a large initial length, say 20 percent of the dam height, so that the update step is large enough. If the solution fails to converge, $\rho$ is halved till the convergence reaches.

However, the strategy is for updating the inner points of the free surface, $Q_1, Q_2, \ldots, Q_s$, but cannot be used to shift the exit point E of the free surface. This is because point E has been given a water head equal to its ordinate prior to solving system (14). In the literature on the adaptive mesh methods, the exit point E is determined by extrapolating the last two points, $Q_{s-1}$ and $Q_s$, on the current free surface, causing the deterioration in precision.

In Section 4 we have pointed out that the real solution has the property that $q_n > 0$ on the whole seepage face except the exit point E. At point E, $q_n = 0$. Using this fact, we can readily locate the exit point E by interpolation or extrapolation to $q_n$. We are justified for doing so because $q_n$ is not calculated by differentiating water head $\phi$ but rather it is another variable independent of $\phi$. As a result, $q_n$ is accurate enough to assure the location of the exit point E is accurate as well.

We mention that Kazemzadeh and Daneshmand [12] also preset some shifting paths so that the distinct points, $Q_1$, $Q_2, \ldots, Q_s$, on the potential free surface, are kept inside $\Omega_w$. On the one hand, however, their adjustment to $Q_1, Q_2, \ldots, Q_s$ is not as sophisticated as in this study. On the other hand, their adjustment to the exit point of the free surface is different from what are described in the above, because in [12] $q_n$ on the potential seepage surface is not an independent variable.

## 7. Illustrative examples

In generating the MLS-based shape functions $\{N_\phi^k(\boldsymbol{r})\}$, the linear basis, $\{1, x, y\}$, is adopted in this study. We also tried the quadratic basis but yielded little differences. The weight function of the $k$th $\phi$-node is defined as

$$w_k(r) = \begin{cases} 1 - 6r^2 + 8r^3 - 3r^4, & \text{if} \quad r < 1 \\ 0, & \text{if} \quad r \ge 1 \end{cases}, \tag{17}$$

with

$$r = \frac{1}{R}\sqrt{(x - x_k)^2 + (y - y_k)^2}.$$

Here, $R$ is radius of the influence domain of the $k$th $\phi$-node and $(x_k, y_k)$ the coordinate of node. Because the linear basis has a dimension of three, $R$ should be large enough such that any point (usually a Gaussian point) in $\Omega$ is contained in the influence domains of at least three $\phi$-nodes that are not in the same line, see [18] for details.

For all the following examples, $\phi$-nodes are evenly deployed in both $x$- and $y$-directions. Denoting by $S$ the span of $\phi$-nodes, we take $R = 2S$. Improvements in precision are limited when $R$ varies between $2S$ and $5S$, but the band width of matrix $\boldsymbol{K}$ increases considerably.

### 7.1. A homogeneous rectangular dam

Shown in Fig. 9 is the cross-section of a homogeneous rectangular dam resting on an impervious layer. This is one of very few examples that have analytical solutions in the unconfined seepage analysis. The analytical solution was given by

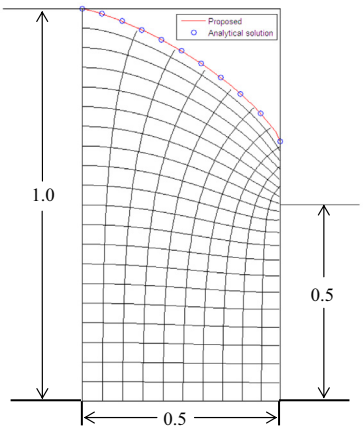


**Fig. 9.** A homogeneous dam ($S = 0.05$).

Polubarinova-Kochina [31] in the elliptic integral form of the first kind, but so complicated in calculation that it was seldom used as a reference to test numerical methods until Hornung and Krueger [32] gave accurate numerical results in a series of tables and graphs.

Fig. 9 also displays the flow net with a $\phi$-nodes span given in the blanket, ($S = 0.05$). Table 1 lists the distinct points on the final free surface, suggesting the proposed solution is in good agreement with the analytical solution.

### 7.2. An inhomogeneous rectangular dam

Shown in Fig. 10 is the configuration of a rectangular dam with two vertical layers resting on an impervious foundation. Since Oden and Kikuch [8], this example has been used as a benchmark by many researchers to test the ability of their numerical methods to treat drastic singularity in the free surface.

This example is also an excellent paradigm to show the necessity to formulate the EFGM in the setting of the NMM, where the free surface takes on drastic singularity. Now we explain this as follows. It can be expected that the free surface will turn

**Table 1**
Coordinates of some points on the free boundary (Ex-1).

| $x$ | $y$ | | $x$ | $y$ | |
|---|---|---|---|---|---|
| | Analytic | Proposed | | Analytic | Proposed |
| 0.00 | 1.000000 | 1.000000 | 0.30 | 0.859969 | 0.859755 |
| 0.05 | 0.986242 | 0.986092 | 0.35 | 0.823876 | 0.823290 |
| 0.10 | 0.967625 | 0.967407 | 0.40 | 0.782493 | 0.782228 |
| 0.15 | 0.945590 | 0.945669 | 0.45 | 0.733142 | 0.732739 |
| 0.20 | 0.920382 | 0.920391 | 0.50 | 0.662382 | 0.659618 |
| 0.25 | 0.891939 | 0.891769 | \ | \ | \ |

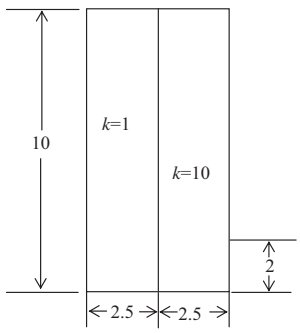


**Fig. 10.** Rectangular dam with two vertical layers.

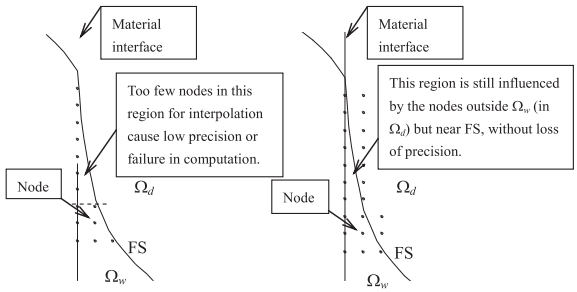


(a) Node configuration in EFG (b) Node configuration in NMM

**Fig. 11.** Node configurations in EFG and NMM.

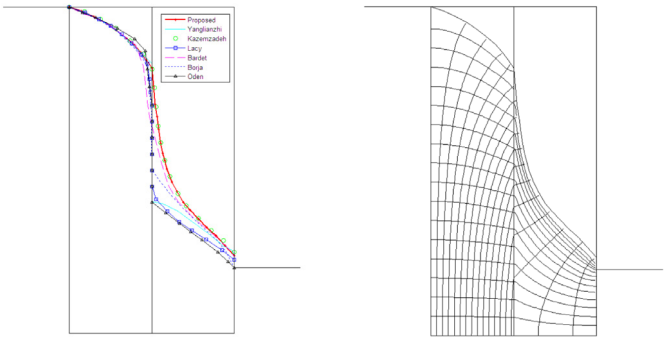


(a) Comparison of free surfaces (b) Flow net of the proposed ($S$=5/12)

**Fig. 12.** Comparison between the proposed and others.

abruptly downward after penetrating through the material interface. If the EFGM is adopted alone, where all relevant nodes match $\Omega_w$, the preset nodes in the narrow region between the material interface and the free surface, see Fig. 11(a), become insufficient to influence the Gaussian points in the narrow region, causing an interrupt in calculating the MLS-based shape functions. In calculating the shape functions at a Gaussian point, as is well known, the MLS requires that the Gaussian point be contained in the influence domains of at least three nodes if the linear basis is adopted. During the solution, in principle we can provisionally add some new nodes into the narrow domain in Fig. 11(a). In practice, however it is by no means an easy errand. On the one hand, these newly added nodes must be in the narrow region but not on the same line, causing the programming laborious. On the other hand, it is absolutely arduous to deploy new nodes within a narrow region so as to assure accuracy and stability. Instead, the NMM presets the nodes throughout $\Omega$ at the best points for the best interpolation precision. During the update of the free surface, some nodes are outside $\Omega_w$, but still those nodes near the free surface can influence the narrow domain, see Fig. 11(b), and occupy the best locations for interpolation. Therefore, the introduction of the NMM to the EFGM simplifies the programming significantly and assures accuracy and numerical stability of solution.

While this example has been solved by so many numerical methods, see Fig. 12 for the positions of the free surface evaluated by different methods, no comparisons have been made between these methods. Now that no analytical solution is available for this example, we here utilize such a fact that the rate of flow quantity through distinct vertical sections in the dam should be equal in theory, as follows

$$Q(x) = \int_0^{y_F} v_x dy = \text{constant},$$

along the axis $x$. Here, $y_F$ = ordinate of the free surface with the abscissa $x$.

Fig. 13 displays the distributions of flow quantity rate along the axis-$x$, which are obtained by regarding the final free surface as the impervious boundary. Fig. 14 shows the same distributions as Fig. 13 but they are obtained by regarding the final free surface as the water head boundary and solving $\delta\pi^2 = 0$. From the two graphs, we can see that the results from Kazemzadeh and Daneshmand [12] and the proposed procedure perform better. Having smoothed the gradient of water head, in order to reach higher precision, Kazemzadeh and Daneshmand [12] accurately calculate the flow matrices of those elements cut by the free surface. This causes the programming to get involved. In this study the calculation of the flow matrices is carried out on the background net. Using the background grid would marginally sacrifice precision in calculating

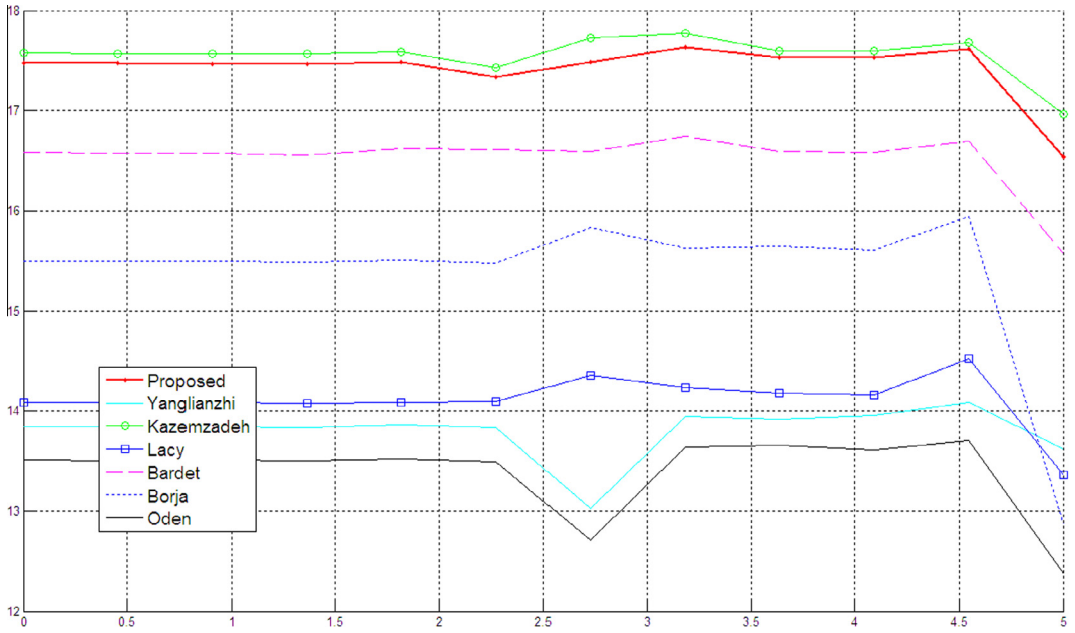


**Fig. 13.** Flow quantity distribution by regarding free surface impervious.

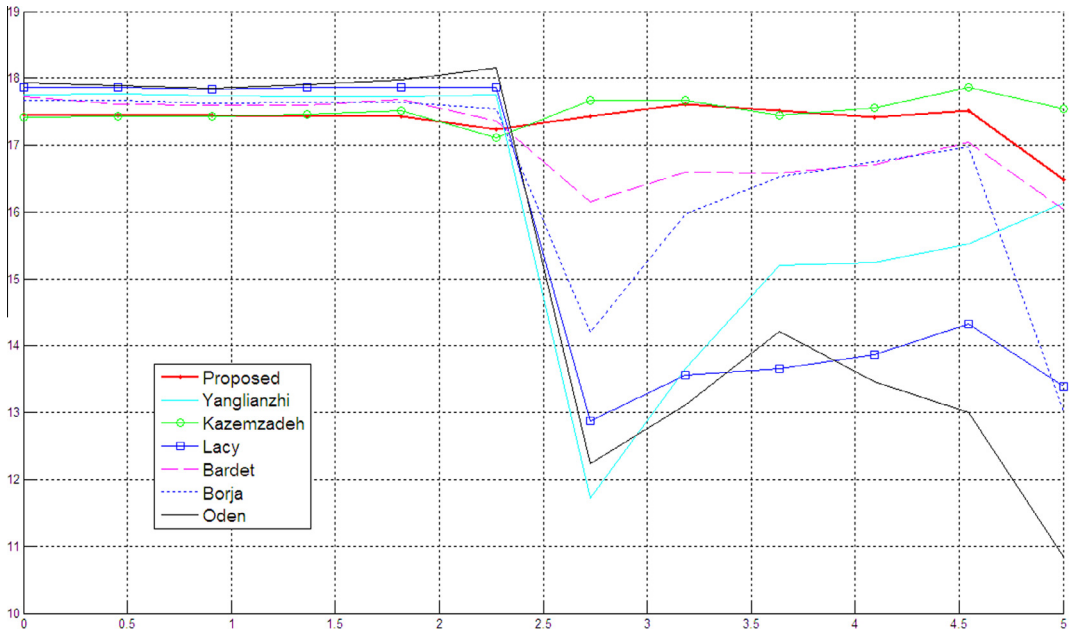


**Fig. 14.** Flow quantity distribution by regarding free surface as water head boundary.

the flow matrices but greatly simplify the programming. Therefore, the combination of the NMM and the EFGM achieves an excellent effect in treating the drastic singularity of the free surface. The flow net is displayed in Fig. 12(b).

### *7.3. A trapezoidal ditch underlain by a drain at a finite depth*

Shown in Fig. 15 is a trapezoidal ditch underlain by a drain at a finite depth, marked by shifting paths of some distinct points on the potential free surface. The example was also analyzed by some researchers, among which is Kazemzadeh and Daneshmand [12].

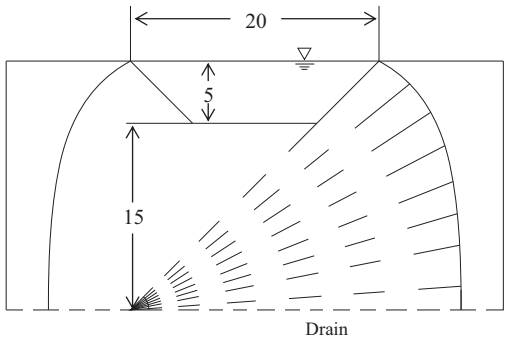


**Fig. 15.** Seepage under a symmetric trapezoidal ditch (unit: ft).

By the classical FEM alone, it is hard to reach a convergent solution to this example. This might be caused by the fact that the free surface is, as a whole, nearly vertical.

Adopting the smoothed finite element method, Kazemzadeh and Daneshmand [12] made great efforts to solve this example, where sophisticated techniques are proposed for suppressing the zigzag of the free surface in iterations.

By the proposed procedure, no particular treatment is taken during iteration. Fig. 16 shows the flow net.

### *7.4. An earth and rockfill dam with sloping core*

Finally, let's consider seepage flow through an earth and rockfill dam with complicated structures of seepage control, including a sloping core and a horizontal drain, see Fig. 17 for details, where the dam rests on a slightly permeable foundation whose bedding plane is inclined to the horizontal.

Seepage control is of utmost importance in the design of earth and rockfill dams. When a sloping central core is built inside the earth and rockfill dam, the seepage analysis is so complicated that all calculations, such as plotting of flow nets and evaluation of flow quantity rate, are based on rough approximations and empirical formulae, see [33] for example.

The difficulties in the seepage analysis of such a dam type are caused by the discontinuity of the free surface. Due to the permeability contrast within the dam, an internal seepage face develops along the interface between the sloping core and the rest behind the core. Because of this, we can anticipate the development of a partially saturated region beneath the overhanging slope. Since the proposed procedure is not designed to treat unsaturated flow, the problem arises as to how much of this flow moves vertically downward to the free surface and how much moves laterally above the saturated zone to the horizontal drain. Neuman and Witherspoon [34] can be consulted for more detailed explanation.

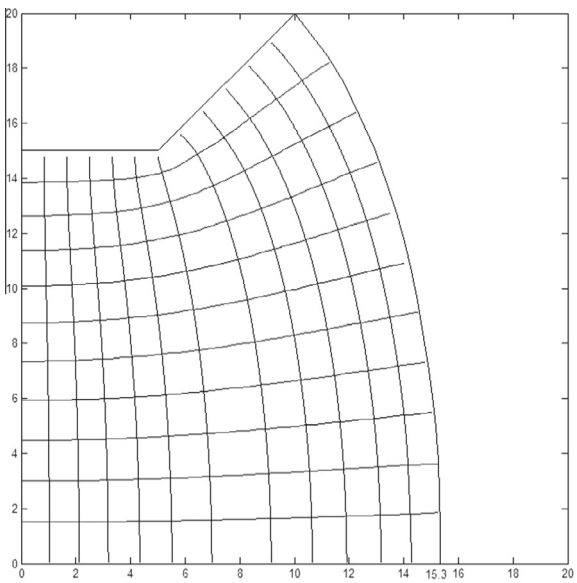


**Fig. 16.** Results of seepage under the trapezoidal ditch ($S = 1$).

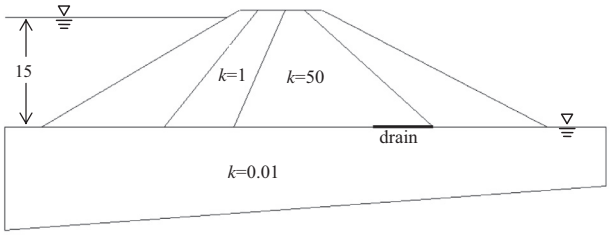


**Fig. 17.** A dam with sloping core and horizontal drain on a slightly permeable foundation.

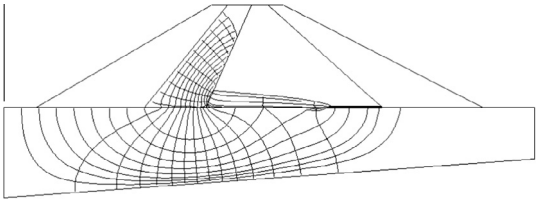

**Fig. 18.** Flow net of the earth and rockfill dam ($S = 2$).

Now we solve this problem by considering all water that flows across the overhanging seepage face is totally lost. The resulting free surface is the lower limit of the actual free surface. Such a treatment is on the safe side in the stress analysis, because the hydraulic gradient in the core is overestimated, causing the seepage force to be overestimated.

It should be noted that in iterations the directions of shifting vary from nearly horizontal along the drain to a direction that is parallel to the interface between the two parts of the dam. Shifting the free surface is done independently in each part of the dam.

Shown in Fig. 18 is the flow net, from which we can see the streamlines are very well perpendicular to the equipotential lines.

## 8. Conclusions

The element-free methods, like the EFGM, are powerful in solving the free boundary problems. However, high accuracy cannot be achieved by simply using the shape functions with the interpolation property; instead, the essential boundary conditions and the interface continuity conditions must be enforced in the sense of the Lagrangian multiplier. The free surface, as well as the seepage point, can be shifted smoothly in iteration by the update strategy proposed in this study. Meanwhile, the EFGM in the framework of the NMM becomes more efficient and more stable in solution, but easier in programming. It is expected that the combination of the EFGM and the NMM is beneficial to solving more complicated free boundary problems.

## Acknowledgments

This study is also supported by the National Basic Research Program of China (973 Program), under the Grant No. 2011CB013505.

## References

[1] C.S. Desai, G.C. Li, A residual flow procedure and application for free surface in porous media, Adv. Water Resour. 6 (1983) 27–35.
[2] H.W. Alt, Numerical solution of steady state porous flow free boundary problems, Numer. Math. 36 (1980) 73–96.
[3] R.I. Borja, S. Kishnani, On the solution of elliptic free-boundary problems via Newton's method, Comput. Methods Appl. Mech. Eng. 88 (1991) 341–361.
[4] C.S. Desai, B. Baseghi, Theory and verification of residual flow procedure for 3-D free surface seepage, Adv. Water Resour. 11 (1988) 192–203.
[5] D.R. Westbrook, Analysis of inequality and residual flow procedures and an iterative scheme for free surface seepage, Int. J. Numer. Methods Eng. 21 (1985) 1791–1802.
[6] H. Zheng, H.C. Dai, D.F. Liu, A variational inequality formulation for unconfined seepage problems in porous media, Appl. Math. Model. 33 (2009) 437–450.
[7] K.J. Bathe, M.R. Khoshgoftaar, Finite element free surface seepage analysis without mesh iteration, Int. J. Numer. Anal. Methods Eng. 3 (1979) 13–22.
[8] J.T. Oden, N. Kikuchi, Theory of variational inequalities with applications to problems of flow through porous media, Int. J. Eng. Sci. 18 (1980) 1173–1284.
[9] J.C. Bruch, Fixed domain methods for free and moving boundary flows in porous media, Transp. Porous Media 6 (1991) 627–649.
[10] H. Zheng, D.F. Liu, C.F. Lee, L.G. Tham, A new formulation of Signorini's type for seepage problems with free surface, Int. J. Numer. Methods Eng. 64 (2005) 1–16.

[11] Y.F. Chen, R. Hu, C.B. Zhou, D.Q. Li, G. Rong, A new parabolic variational inequality formulation of Signorini's condition for non-steady seepage problems with complex seepage control systems, Int. J. Numer. Anal. Methods Geomech. 35 (2011) 1034–1058.
[12] M.J. Kazemzadeh-Parsi, F. Daneshmand, Unconfined seepage analysis in earth dams using smoothed fixed grid finite element method, Int. J. Numer. Anal. Methods Geomech. 36 (2012) 780–797.
[13] M. Darbandi, S.O. Torabi, A moving-mesh finite-volume method to solve free-surface seepage problem in arbitrary geometries, Int. J. Numer. Anal. Methods Geomech. 31 (2007) 1609–1629.
[14] J.P. Bardet, T. Tobita, A practical method for solving free-surface seepage problems, Comput. Geotech. 29 (2002) 451–475.
[15] J.Y. Zhang, B. Jiang, Enhanced Euler's method to a free boundary porous media flow problem, Numer. Methods Partial Differ. Equ. 28 (2012) 1558–1573.
[16] M.I. Herreros, M. Mabssout, M. Pastor, Application of level-set approach to moving interfaces and free surface problems in flow through porous media, Comput. Methods Appl. Mech. Eng. 195 (2006) 1–25.
[17] G.X. Li, J.H. Ge, Y.X. Jie, Free surface seepage analysis based on the element-free method, Mech. Res. Commun. 30 (2003) 9–19.
[18] P. Lancaster, K. Salkauskas, Surfaces generated by moving least squares methods, Math. Comput. 155 (1981) 141–158.
[19] G.H. Shi, Manifold method of material analysis, in: Transactions of the 9th Army Conference on Applied Mathematics and Computing, Report No. 92–1, US Army Research Office, Minneapolis, MN, 1991, pp 57–76.
[20] M. Spivak, Calculus on Manifolds, Benjamin, New York, 1965.
[21] I. Babuška, J.M. Melenk, The partition of unity method, Int. J. Numer. Methods Eng. 40 (1997) 727–758.
[22] H. Zheng, Z.J. Liu, X.R. Ge, Numerical manifold space of Hermitian form and application to Kirchhoff's thin plate problems, Int. J. Numer. Methods Eng. 95 (2013) 721–739.
[23] G.W. Ma, X.M. An, L. He, The numerical manifold method: a review, Int. J. Comput. Methods 7 (2010) 1–32.
[24] K. Terada, M. Asai, M. Yamagishi, Finite cover method for linear and non-linear analyses of heterogeneous solids, Int. J. Numer. Methods Eng. 58 (2003) 1321–1346.
[25] H. Zheng, D.D. Xu, New strategies for some issues of numerical manifold method in simulation of crack propagation, Int. J. Numer. Methods Eng. 97 (2014) 986–1010.
[26] A. Shamsai, T.N. Narasimhan, A numerical investigation of free surface – seepage face relationship under steady state flow conditions, Water Resour. Res. 27 (1991) 409–421.
[27] J.Y. Parlange, W. Brutsaert, A capillarity correction for free surface flow of groundwater, Water Resour. Res. 23 (1987) 805–808.
[28] T. Belytschko, Y.Y. Lu, L. Gu, Element-free Galerkin methods, Int. J. Numer. Methods Eng. 37 (1994) 229–256.
[29] J. Aalto, Singularity elements for seepage analysis, Int. J. Numer. Anal. Methods Geomech. 9 (1985) 185–196.
[30] H. Zheng, J.L. Li, A practical solution for KKT systems, Numer. Algorithms 46 (2007) 105–119.
[31] P. Polubarinova-Kochina, Theory of Ground Water Movement, Princeton University Press, Princeton, 1962.
[32] U. Hornung, T. Krueger, Evaluation of the Polubarinova-Kochina formula for the dam Problem, Water Resour. Res. 21 (1985) 395–398.
[33] C.H. Zhang, G.L. Wang, F. Jing, Hydraulic Structures, Tsinghua University Press, Beijing, 2011.
[34] S. Neuman, P. Witherspoon, Finite element method of analyzing steady seepage with a free surface, Water Resour. Res. 6 (1970) 889–897.